An insight into the properties of heteroleptic metal dithiolenes: Multi-Stimuli Responsive Luminescence, Chromism and Nonlinear optics

Salahuddin S. Attar,[a,†] Luca Pilia,[b] Davide Espa,[a,‼] Flavia Artizzu,[c] Angela Serpe,[d] Maddalena Pizzotti,[e] Daniele Marinotto,[f] Luciano Marchiò,*[g] and Paola Deplano*[a,‡]*

[a] Department of Chemical and Soil Sciences, INSTM Research Unit, University of Cagliari, 09042 Monserrato (CA) (Italy)

[b] Dipartimento di Ingegneria Meccanica, Chimica e dei Materiali, Università di Cagliari, Via Marengo 2, 09123 Cagliari (Italy).

[c] L3-Luminescent Lanthanide Lab, Department of Chemistry, Ghent University

Krijgslaan 281-building S3, B-9000 Gent (Belgium)

[d] Dipartimento di Ingegneria Civile, Ambientale e Architettura, INSTM Research Unit, Università di Cagliari, Via Marengo 2, 09123 Cagliari (Italy)

[e] Department of Chemistry, INSTM Research Unit, University of Milan

Via C. Golgi 19, 20133 Milano (Italy)

[f] CNR-SCITEC, Centro di eccellenza CIMAINA, Via C. Golgi 19, 20133 Milano (Italy)

[g] Dipartimento SCVSA, Università di Parma, Parco Area delle Scienze 17/a, 43124, Parma (Italy).

ABSTRACT. A comprehensive investigation of the functional properties of heteroleptic Donor-M-Acceptor dithiolene Bu4N[M^{II}(L1)(L2)] complexes is presented (M = Pd, Pt). The acceptor L1 consists in the chiral (*R*)-(+)α-methylbenzyldithio-oxamidate: (*R*)-*α*-MBAdto; the donor L2 is the 2-thioxo-1,3-dithiole-4,5-dithiolato (dmit) in **1** (Pd), and **2** (Pt), the 1,2-dicarbomethoxyethylene dithiolate (ddmet) in **3** (Pd), and **4** (Pt), or the[4′,5′:5,6][1,4]dithiino[2,3-b]quinoxaline-1′,3′dithiolato (quinoxdt) in **5** (Pd), and **6** (Pt). L1 is capable to undergo proton exchange and to promote crystals formation in noncentrosymmetric space groups. L2 has different molecular structures while maintaining similar electrodonating capability. Thanks to the ligands' synergy, **1-6** behave as H^+ and Ag^+ switchable linear chromophores. Moreover, the compounds exhibit H^+-switchable second-order NLO response in solution, which is maintained in the bulk for **1**, **3** and **4** when embedded into PMMA poled matrix. **5** and **6** show unique anti-Kasha H^+ and Ag^+ tunable colored emission originating from the quinoxdt ligand. The correlation between the electronic structure and properties is performed through Density Functional Theory (DFT) and time-dependent DFT calculations.

KEYWORDS Donor acceptor systems; X-ray diffraction; Fluorescence; Nonlinear optics; Density Functional Calculations

Introduction

The interest in metal dithiolene chemistry in basic science[1,2] and in various fields of materials chemistry,[3-5] has been fueled by the growing attention to heteroleptic derivatives with potential application in dyes-sensitized solar cells[6-8] or in second-order nonlinear optics (NLO).[9-10] Following well established engineering,[11] these complexes can be obtained as planar and low-energy-gap molecules consisting of a π-acceptor (A) and a π-donor (D) ligand connected by a d^8-metal in a square-planar coordination, where the metal acts as a suitable π-bridge for the D-A charge transfer (CT) transition. Several other class of complexes, where a d8-metal (mostly platinum) connects a variety of suitably engineered D-A ligands, are of interest for their NLO and photoemissive properties as well as in photocatalysis.[12] It seems worth to remind that the term dithiolene is commonly employed irrespective of the real form of the ligand in a particular complex, in which the ligand is capable to bind metals as ene-1,2-dithiolate dianion, mixed-valence thioketone-radical thiolate monoanion, neutral dithioketone, depending on the electron-withdrawing/donating properties of substituents at the C2S2 moiety. Indeed, the substituents affect the energy of the frontier molecular orbitals (MOs) and thus the formal oxidation state for the ligand, which spans from 2- (electronwithdrawing substituents, such as CN) to 0 (electron donating ones, such as NR_2), Figure 1.[13] Accordingly, heteroleptic d^8 metal dithiolenes with proper substituents at the C2S2 moieties, behave as D-M-A molecules with a non-null dipolar moment. In these D-M-A compounds, the CT process produces a decrease of the dipole moment from the ground to the excited state, giving rise to negative solvatochromism and first hyperpolarizability (β), see Figure 1. The first hyperpolarizability is related to the way the mobile electronic charges respond to the oscillating electric field of a laser beam, hence generating second-order NLO effect at the molecular level.[14a] To translate second order NLO activity to the bulk, the lack of an inversion center is required while the formation of centrosymmetric assemblies of molecules due to antiparallel alignment of dipolar D-A units, is

detrimental. Different strategies can be employed to maintain NLO response in the bulk. In particular, a strategy implies the use of enantiomerically pure-substitutents in the D-A systems to ensure the formation of crystals in noncentrosymmetric space groups. A second strategy comprises the formation of poled polymers, where the required asymmetry is imposed by the external electric field.[14b]

Further tuning of linear and non-linear optical properties of these systems can be achieved through the fine modulation of the ligands. The bottom-up tailoring allows to expand their properties by integrating specific functional groups capable to respond to external stimuli[15,16] (protons, metal ions, light-irradiation). Hence, the modulation of the D-A systems by chemical synthesis allows to achieve multi-responsive chromophores with potential use as sensors[17] or for other smart multifunctional devices.[18]
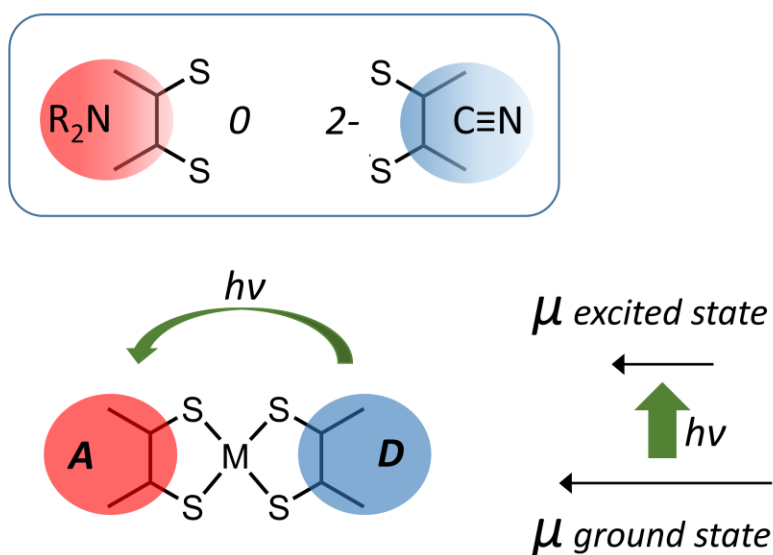
Figure 1. Depiction of the electronic properties of the dithiolene ligands and of the D-M-A complexes. Above, pictorial description of the formal charges as a function of the substituents. Below, variation of the dipole moment (μ, $\rightarrow$) during the charge transfer.

In this context, we report here a study on heteroleptic Pd[II] and Pt[II] dithiolene complexes where ligands were designed to achieve multi-responsive optical properties. As far as the acceptor is concerned, we focused on the (R)-(+)-α-Methyl benzyl dithio-oxamidate [(R)-α-MBAdto = L1] since it is able to promote a remarkable proton-switchable linear[19] and nonlinear optical[20a] response. Moreover, this ligand presents homochiral stereo-centers, and it guarantees the crystallization of the compounds in non-centrosymmetric space groups, which is a necessary but not sufficient requisite to achieve a SHG (Second Harmonic Generation) response in the bulk.[21,22] On the other hand, the donor ligands, with similar electron donating (R2) capability, are based on a C2S2 moiety functionalized with i) a condensed heterocycle in **1** and **2** (dmit = 2-thioxo-1,3-dithiole-4,5-dithiolato), ii) two conformationally flexible ester groups in **3** and **4** (ddmedt = dicarbomethoxyethylene dithiolato), and iii) a thioether bridge connecting a quinoxaline ring in **5** and **6** (quinoxdt = [4',5':5,6][1,4]dithiino[2,3-b]quinoxaline-1',3'dithiolato). This will allow to elucidate the role of the different molecular structures of the donor in affecting the properties of related complexes, with particular attention to quinoxdt in promoting luminescent anti-Kasha behaviour, unique among this class of Pt and Pd dithione-dithiolate complexes.[20,23] Experimental and computational studies are here presented to highlight the factors affecting the properties of these functionalized D-M-A linear and NLO-chromophores to achieve multiresponsive properties.

Experimental Section

   Synthesis of Products

Reagents and solvents were purchased from Aldrich and used without further purification. (*R*)-α-MBAdto was synthesized according to a literature method[24] and obtained in a 60% yield. Precursors and products shown in Scheme 1 are prepared and characterized as follows.

[Pd((R)-α-MBAdto)(DMSO)Cl]. A solution of [Pd(DMSO)$_2$Cl$_2$] (250 mg, 0.75 mmol) in 20 mL of MeOH was added portion wise to a solution of (R)-α-MBAdto (246.1mg, 0.75 mmol) in 130mL CHCl$_3$. The orange-yellow solution obtained was then stirred overnight at room temperature. Orange-yellow powder of [Pd((R)-α-MBAdto))(DMSO)Cl] (392 mg, yield 95%) was collected by centrifugation. The product was used for the next step without further purification. Elemental Analysis: calculated for C$_{20}$H$_{25}$ClN$_2$OPdS$_3$ (547.49): C, 43,88; H, 4.60; N, 5.12; found: C, 44.11; H, 4.31; N, 5.41. FT–IR (KBr): ν_{max} cm^{-1}:3193 (s); 3090 (s); 2980 (m); 2925 (m);1568 (vs); 1529 (m); 1494 (w); 1447 (m); 1430 (vs); 1384 (s); 1347 (w); 1326 (w); 1214 (w); 1188 (m); 1087 (m); 1022 (w); 980 (vw); 915 (vw); 840 (vw); 760 (m); 698 (s), 540 (w)

***n*-Bu$_4$N[Pd((R)-α-MBAdto)(dmit)] (1).** A solution of Na (9.2 mg, 0.4 mmol) in 15 mL of MeOH was added drop wise to a stirred suspension of [1,3]dithiolo[4,5-d]dithiole-2-one-5-thioxo (C$_4$S$_5$O) (44.8 mg, 0.20 mmol) in 50 mL 50% MeOH/CHCl$_3$. The mixture was stirred for 30 min at room temperature. The dithiolate solution was then added drop wise to a yellow solution of [Pd((R)-α-MBAdto)(DMSO)Cl] (110 mg, 0.20 mmol) in 120 mL 20% MeOH/CHCl$_3$ at room temperature; the reaction mixture was stirred overnight and the solution turned to blue-purple. The obtained mixture was filtered, and the solvent evaporated to a 1/4th of the initial volume. Afterwards, a solution of Bu$_4$NBr (96.5 mg, 0.3 mmol) in MeOH was added drop-wise and the resulting mixture was roto-evaporated to dryness. The solid product was dissolved in 20 mL of CH$_3$CN and filtered through a cotton plug directly into a crystallization vessel. Crystals were obtained by recrystallization in CH$_3$CN/diethyl ether (133 mg, 0.13 mmol; yield 65%). Analytical results are in accordance with the formula *n*-Bu$_4$N[Pd((R)-α-MBAdto)(dmit)].

Elemental Analysis: calculated for $C_{37}H_{55}N_3PdS_7$ (872.73): C, 50.92; H, 6.35; N, 4.81; found: C, 50.61; H, 6.52; N, 4.66. UV-Vis (DMF solution): λ_{max} (nm), ε (molcm^{-1}dm^{-3}): 525, 1.57x10^4; FT–IR (KBr): ν_{max} cm^{-1}: 3190 (m); 3022 (vw); 2962 (m); 2869 (w); 1636 (m); 1516 (s); 1454 (s); 1377 (m); 1342 (w); 1300 (w); 1205 (vw); 1163 (w); 1130 (w); 1051 (vs); 1026 (m); 898 (w); 761 (m); 700 (m); 659 (vw); 554 (w); 516 (vw); 485 (vw).

n-Bu₄N[Pt((R)-α-MBAdto)(dmit)] (2). This complex was prepared following the same procedure reported above for **1** using 192 mg of [Pt(R)-α-MBAdto)(DMSO)Cl] (0.20 mmol) in 120mL 20% MeOH/CHCl$_3$ at room temperature (106 mg, 0.10 mmol; yield 55%). Analytical results are in accordance with the formula n-Bu₄N[Pt((R)-α-MBAdto)(dmit)]. Elemental Analysis: calculated for $C_{37}H_{55}N_3PtS_7$ (961.39): C, 46.22; H, 5.77; N, 4.37; found: C, 46.39; H, 5.52; N, 4.22. UV-Vis (DMF solution): λ_{max} (nm) ε (mol cm^{-1}dm^{-3}): 344, 1.25x10^4; 543, 9.68x10^3; FT–IR (KBr): ν_{max} cm^{-1}: 3209 (m); 3051 (vw); 2960 (m); 2869 (w); 1649 (m); 1500 (vs); 1452 (s); 1378 (w); 1343 (m); 1173 (w); 1131 (vw); 1053 (vs); 1027 (s); 906 (w); 759 (w) 699 (m); 549 (vw); 515 (vw); 467 (vw).

n-Bu₄N[Pd((R)-α-MBAdto)(ddmedt)]·1/2H₂O (3). Na (13.8 mg, 0.6mmol) was added to 22 mL of MeOH; the resulting solution was drop wise to a stirred suspension of 4,5-dicarbomethoxy-1,3-dithiol-2-one (70.2 mg, 0.30 mmol) in 60 mL 50% MeOH/CHCl$_3$. The mixture was stirred for 30 min at room temperature. The dithiolate solution was then added drop wise to a yellow solution of [Pd((R)-α-MBAdto)(DMSO)Cl] (167.0 mg, 0.30 mmol) in 150 mL 20% MeOH/CHCl$_3$ at room temperature; the reaction mixture was stirred overnight and the solution turned to red-orange. The obtained mixture was filtered, and the solvent evaporated to a 1/4th of the initial volume. Afterwards, a solution of Bu₄NBr (145.2 mg, 0.45 mmol) in MeOH was added drop wise and the resulting mixture was roto-evaporated to dryness. The solid product was dissolved in ca. 20 mL of CH$_3$CN and filtered through a cotton plug directly into a

crystallization vessel. The solid obtained in CH_3CN/diethyl ether was dissolved in MeOH, and for slow evaporation a microcrystalline powder was obtained (194 mg, 0.22 mmol; yield 73%). Analytical results are in accordance with the formula $Bu_4N[Pd((R)-\alpha$-MBAdto)(ddmedt)]·$1/2H_2O$. Elemental Analysis: calculated for $C_{40}H_{62}N_3O_{4.5}PdS_4$ (891.62); C, 53.88; H, 7.01; N, 4.71; found: C, 54.12; H, 7.02; N, 4.49. UV-Vis (DMF solution): λ_{max} (nm) ε (molcm^{-1}dm^{-3}): 390, 4.76x10^3; 525, 4.46x10^3; FT–IR (KBr): ν_{max} cm^{-1}: 3210 (m) 3025 (vw); 2961 (m); 2871 (w); 1720 (s); 1698 (s); 1681 (s); 1650 (m); 1514 (vs); 1454 (m); 1429 (w); 1379 (w); 1322 (w); 1228 (vs); 1162 (w); 1102 (vw); 1073 (w); 1034 (m); 883 (vw); 745 (m); 710 (m); 491 (vw).

n-Bu$_4$N[Pt((R)-α-MBAdto)(ddmedt)]·$1/2H_2O$ (4). Complex **4** was prepared following the same procedure reported above for **3** using 288 mg of [Pt((R)-α-MBAdto)(DMSO)Cl] (0.30 mmol) in 150mL 20% MeOH/CHCl$_3$ at room temperature (194 mg, 0.20 mmol; yield 66%). Single crystals suitable for X-ray diffraction measurements were obtained by slow evaporation of a MeOH solution corresponding to n-Bu$_4$N[Pt((R)-α-MBAdto)(ddmedt)]·$1/2H_2O$, **4**. Elemental Analysis: calculated for $C_{40}H_{62}N_3O_{4.5}PtS_4$ (980.28); C, 49.01; H, 6.37; N, 4.29; found: C, 49.78; H, 6.54; N, 4.10. UV-Vis (DMF solution): λ_{max} (nm) ε (mol cm^{-1}dm^{-3}): 392, 3.97x10^3; 603, 5.29x10^3; FT–IR (KBr): ν_{max} cm^{-1}: 3208 (m); 3028 (vw); 2964 (m); 2872 (w); 2834 (vw); 1691 (s); 1633 (ms); 1522 (vs); 1454 (vs); 1378 (w); 1323 (w); 1226 (vs); 1182 (m); 1132 (m); 1086 (m); 1024 (m); 908 (vw); 797 (vw); 743 (m); 697 (m); 565 (w).

n-Bu$_4$N[Pd((R)-α-MBAdto)(quinoxdt)] (5) Na (9.2 mg, 0.4mmol) was added to 15 mL of MeOH; the resulting solution was drop wise to a stirred suspension of [1,3]dithiolo[5,6][1,4]dithiino[2,3-b]quinoxaline-2-one (59.1 mg, 0.18 mmol) in 50mL 50% MeOH/CHCl$_3$. The mixture was stirred for 30 min at room temperature to obtain a reddish-brown dithiolate solution. The dithiolate solution was then added drop wise to a yellow solution

of [Pd((R)-αMBAdto)(DMSO)Cl] (100 mg, 0.18 mmol) in 120 mL 20% MeOH/CHCl$_3$ at room temperature. The reaction mixture was stirred overnight, and the solution turned to red-purple. The obtained mixture was filtered, and the solvent evaporated to a 1/4th of the initial volume. Afterwards, a solution of *n*-Bu$_4$NBr (117.5 mg, 0.37 mmol) in MeOH was added drop wise and the resulting mixture was roto-evaporated to dryness. The solid product was dissolved in ca. 15 mL of CH$_3$CN and filtered through a cotton plug directly into a crystallization vessel. Dark red crystals (93 mg, 0.097 mmol; yield 54 %) were obtained by recrystallization in CH$_3$CN/diethyl ether. Analytical results are in accordance with the formula *n*-Bu$_4$N[Pd((R)-αMBAdto)(quinoxdt)]. Elemental Analysis: calculated for C$_{44}$H$_{59}$N$_5$PdS$_6$ (956.78): C 55.23; H 6.22; N 7.32; found: C 55.02; H 6.10; N 7.11. UV-Vis (DMF solution): λ$_{max}$ (nm) ε (molcm^{-1}dm^{-3}): 373 (1.37×10^4); 548 (4.57×10^3) FT–IR (KBr): ν$_{max}$ cm^{-1}:3204 (w); 3060 (vw); 3026 (vw); 2961 (m); 2927 (m); 2873 (w); 1508 (vs); 1495 (s); 1479 (s); 1450 (s);1382 (s); 1327 (w); 1303 (w); 1257 (s); 1174 (s); 1111 (s); 1015 (m); 909 (w); 865 (m); 758 (s); 699 (s); 658 (m); 597 (w); 550 (vw).

Measurements

IR spectra (4000−400 cm^{-1}) were recorded with a Bruker Tensor 27 Platinum ATR. Electronic absorption spectra were recorded with an Agilent Cary 5000 spectrophotometer. Elemental analyses were performed by means of a Carlo Erba CHNS Elemental Analyzer Model EA1108.

Experimental single-crystal X-ray analysis.

A summary of data collection and structure refinement for *n*-Bu$_4$N[Pd(L1)(dmit)] (**1**), *n*-Bu$_4$N[Pt(L1)(dmit)] (**2**), *n*-Bu$_4$N[Pt(L1)(ddmedt)]·1/2H$_2$O (**4**) and [Pd(L1)(quinoxdt)] (**5**) is reported in Table S1. Single crystal data were collected with Bruker CCD APEXII and Breeze diffractometers and with a Bruker D8 equipped with a PhotonII area detector (Mo Kα: λ = 0.71073 Å. The data collection strategy was set in order to cover the sphere of the reciprocal

space.[25] Absorption correction was applied using the program SADABS.[26] The structures were solved by direct methods (SIR2011)[27] and with the SHELXT code[28] and refined with ShelXL[29] using Least Squares minimisation. Graphical material was prepared with the Mercury program.[30] CCDC 2013138-2013141 contain the crystallographic data for the compounds.

Computational Details.

The electronic properties of the $[M(L1)(L2)]^-$ complexes (M = Pd, Pt) were investigated by means of DFT methods.[31] All the calculations were performed with the Gaussian 16 program suite.[32] The molecular structures of $[Pd(L1)(dmit)]^-$ (**1a**), $[Pt(L1)(dmit)]^-$ (**2a**), $[Pt(L1)(ddmedt)]^-$ (**4a**), $[Pd(L1)(quinoxdt)]^-$ (**5a**), and $[Pt(L1)(quinoxdt)]^-$ (**6a**), were optimized starting from the X-ray experimental geometry without symmetry constraints. The $[Pt(L1)(quinoxdt)]^-/2(AgCF_3SO_3)$ adduct was optimized starting from a molecular model in which the silver cations were located above and below the PtS_4 coordination plane. The Becke three-parameter exchange functional with Lee-Yang-Parr correlation functional (B3LYP)[33,34] was employed together with the 6-31+G(d) basis set[35,36] for the C, H, N, and S atoms. The Pt, Pd, and Ag atoms were treated with the SDD valence basis set[37,38,39] and with the MWB28 (Pd, Ag), and MWB60 (Pt) effective core potentials. The calculations were performed by using the polarizable continuum model (PCM)[40] to address solvation effects (N,N-dimethylformamide). The first twenty singlet-singlet vertical excitation energies of the optimized complexes were determined using time-dependent density functional theory (TD-DFT)[41,42] at the same level of theory of the geometry optimization. AOMix was used for determining atomic orbital compositions employing Mulliken population analysis.[43]

Photoluminescence.

Measurements were performed using an Edinburgh FLSP920 spectrophotometer equipped with a Hamamatsu R928P PMT detector (200 – 900 nm). Steady-state PL spectra were acquired

using a 450W continuous- wave (CW) xenon lamp as excitation source. Appropriate optical filters were used, and steady-state measurements were corrected for detector response.

Second-order Nonlinear Optical Properties.

The second order NLO responses of the molecular chromophore was measured by the EFISH technique, which provides the γ_{EFISH} value, from which EFISH quadratic hyperpolarizability β_λ can be obtained through equation below

$$\gamma_{EFISH} = (\mu\beta_\lambda/5KT) + \gamma(-2\omega;\omega,\omega,0)$$

where μ is the ground state dipole moment, $\mu\beta_\lambda/5kT$ the dipolar orientational contribution, λ is the fundamental wavelength of the incident photons in the EFISH experiment, $\gamma(-2\omega;\omega,\omega,0)$ is a third-order term at frequency ω of the incident photons, corresponding to the cubic contribution to γ_{EFISH}, usually negligible for dipolar chromophores such as the one studied in this work. Finally, β_λ is the projection along the dipole moment axis of the vectorial component β_{VEC} of the tensorial quadratic hyperpolarizability. In the following, β_λ is reported as β_{1907} since the EFISH experiments were carried out working with a 1907 nm non resonant incident wavelength. All the EFISH measurements were carried out in $CHCl_3$ solutions at 10^{-3} M concentration. The experimental $\mu\beta_{1907}$ values obtained are averaged over 16 measurements.

EFISH measurements.

The compound was first dissolved in $CHCl_3$ at 10^{-3} M concentration and then exposed few minutes to HCl vapours, which led to the formation of the protonated form. The reverse transformation could be induced by the treatment of the protonated compounds with NH_3 vapours for a few minutes. The time required for the protonation and deprotonation processes is related to the solution concentration, higher concentrations requiring longer time exposure to acid/base vapours. The protonation/deprotonation was easily monitored by absorption spectroscopy. All the measurements were carried out in $CHCl_3$ solutions, working with a

nonresonant incident wavelength of 1907 nm, using a Q-switched, mode-locked Nd^{3+}: YAG laser [pulse durations of 15 ns (90 ns) at a 10 Hz repetition rate], manufactured by Atalaser. The 1064 nm initial wavelength was shifted to 1907 nm by a Raman shifter with a high-pressure H_2 cell; the apparatus for the EFISH measurements was made by SOPRA (France).

Kurtz-Perry measurements.

SHG intensity measurements were carried out by the Kurtz–Perry powder technique using a nanosecond Nd:YAG pulsed (10 Hz) laser. The radiation at 1.907 μm was used as the fundamental beam for SHG. The SHG signal was detected by a photomultiplier and compared with a urea standard. The powders were put in a capillary tube.

Polymer film: preparation and characterization.

Composite thin films of **1**, **3** and **4** in Poly(methyl methacrylate) (PMMA, $\bar{M}_w \sim 15000$; $T_g =$ 86.5 °C as determined by differential scanning calorimetry) were deposited by spin-coating (Cookson Electronic Company P-6708D Spin-coater, spinning parameters: RPM1 = 800; ramp1 = 1 s; time1 = 1 s; RPM2 = 2200; ramp2 = 1 s; time2 = 51 s) on a glass slide substrate. Sample solutions were prepared in dichloromethane keeping 5 wt% of **1**, **3** and **4** complexes with respect to PMMA. The thickness of **1**, **3** and **4** films was measured by α-step stylus profilometer (Bruker DektakXT) to be 830.00 ± 21.58 nm, 810.00 ± 21.06 nm and 700.00 ± 18.20 nm, respectively. Protonation on thin films of **1**, **3** and **4** were performed exposing the films to vapors of HCl (34 %). The exposure times of the films varied from a minimum of one hour to a maximum of one day.

Corona-wire Poling Setup.

The fundamental incident light was generated by a 1064 nm Q-switched Nd:YAG (Quanta System Giant G790−20) laser with a pulse of 7 ns and 20 Hz repetition rate. The output pulse was attenuated to 0.50 mJ and focused with a lens (f = 600 mm) on the sample, placed over the hot stage. The corona poling process was performed inside a drybox in a N_2 atmosphere. The

fundamental beam was polarized in the incidence plane (so-called p-polarized) with an angle of about 55° with respect to the sample in order to optimize the SHG signal. The hot-stage temperature was controlled by a GEFRAN 800 controller, while the corona-wire voltage (up to 10 kV across a 10 mm gap) was applied by a TREK 610E high voltage supply. After rejection of the fundamental beam by an interference filter and a glass cutoff filter, the p-polarized SHG signal at 532 nm was detected with a UV−vis photomultiplier (PT, Hamamatsu C3830). The output signal from the PT was set to a digital store oscilloscope and then processed by a computer with dedicated software.

Maker fringe measurement.

In the Maker fringe experiment, the second harmonic intensity was detected as a function of the incidence angle θ of the fundamental beam and normalized with respect to that of a calibrated quartz crystal wafer (X-cut) 1 mm thick whose d_{11} is 0.46 pmV^{-1}. In order to determine the nonzero independent components of the susceptibility tensor ($\chi_{ij}^{(2)}$) for poled films ($C_{\infty v}$ symmetry), Maker fringe measurements were conducted with different polarizations of the fundamental and second harmonic beam: p → p, s → p, and 45° → s (where p and s indicate the polarization of the beam in the plane parallel and orthogonal to the incident one, respectively).[44,45,46]

Results and Discussion

Scheme 1 shows the synthetic approach and the chemical structures for the series of Bu$_4$N[M(L1)(L2)] complexes **1-6**. Compound **6** was described in a previous communication,[20a] and here an extension of studies on its properties is reported. Crystals suitable for single-crystal X-ray diffraction analysis were obtained for **1, 2, 4** and **5**. The details on the synthesis and X-ray characterization are provided in the Experimental Section.
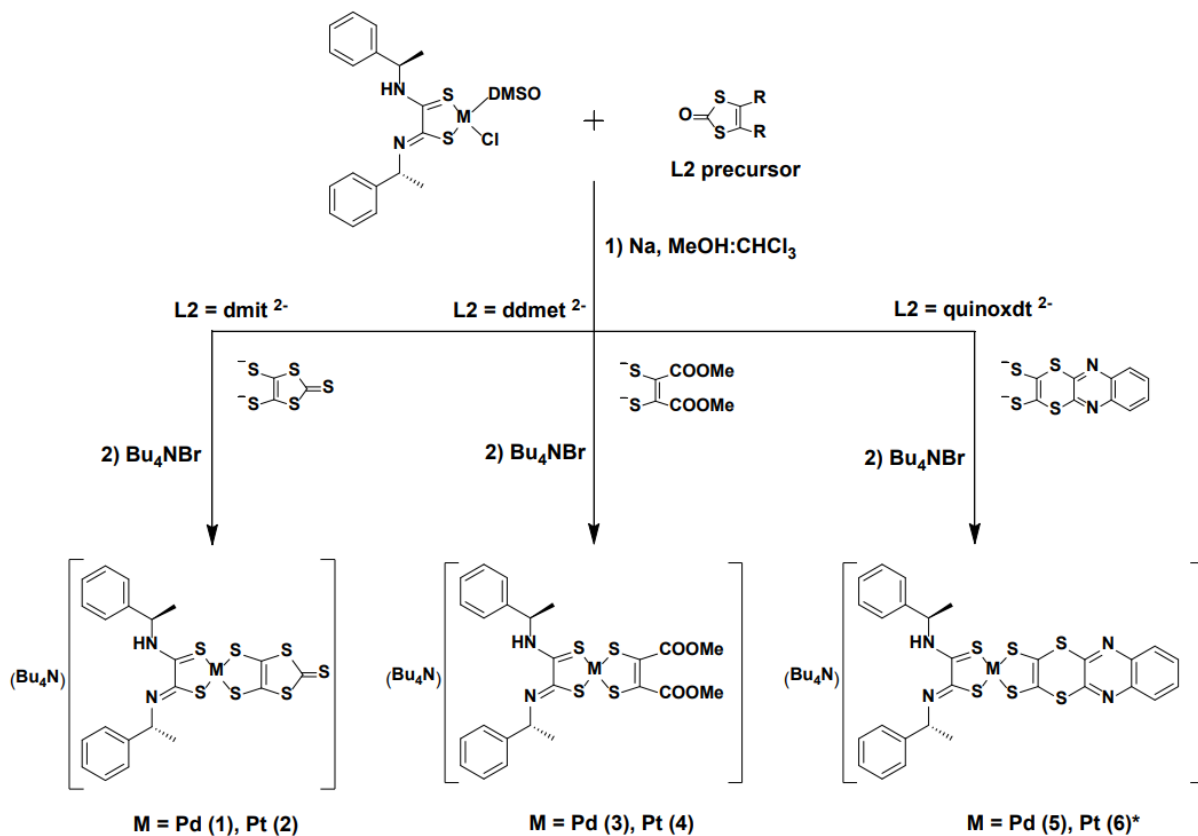
Scheme 1. Depiction of the synthetic procedure together with the molecular structures. **6*** previously reported in reference 20a.

A summary of data collection and structure refinement for Bu₄N[Pd(L1)(dmit)] (**1**), Bu₄N[Pt(L1)(dmit)] (**2**), Bu₄N[Pt(L1)(ddmet)]·1/2H2O (**4**) and Bu₄N[Pd(L1)(quinoxdt)] (**5**) is reported in Table S1. In all compounds, the metal is in a square-planar geometry and it is bound to four sulphur atoms from two different ligands, Figure 2. All the compounds crystallize in non-centrosymmetric and chiral space groups, namely $P2_12_12_1$ for **1**, **2**, and **5**, and $P1$ for **4**. The molecular structures of **1** and **2** are very similar even though not isostructural. For both compounds, the analysis of the crystal packing shows the anion and cations arranged in an alternate fashion along the b crystallographic axis. In **4**, two molecular entities are present, which are linked by a water molecule of crystallization by means of two hydrogen bonds with the peripheral carbonyl group of the ddmet ligands. Along the c axis, the [Pt(L1)(ddmet)]⁻ molecules

are facing each other in an alternate mode through the peripheral fragments of the (*R*)-α-MBAdto and of the ddmet ligands. The Bu_4N^+ cations are interposed between different planar complex molecules. **5** is isostructural to the previously reported Pt analog **6**.[20a] Interestingly, the crystal packing of **5** is similar to that of **4** and the complex molecules interact with symmetry related ones by using the same ligand fragments between symmetry related molecules.
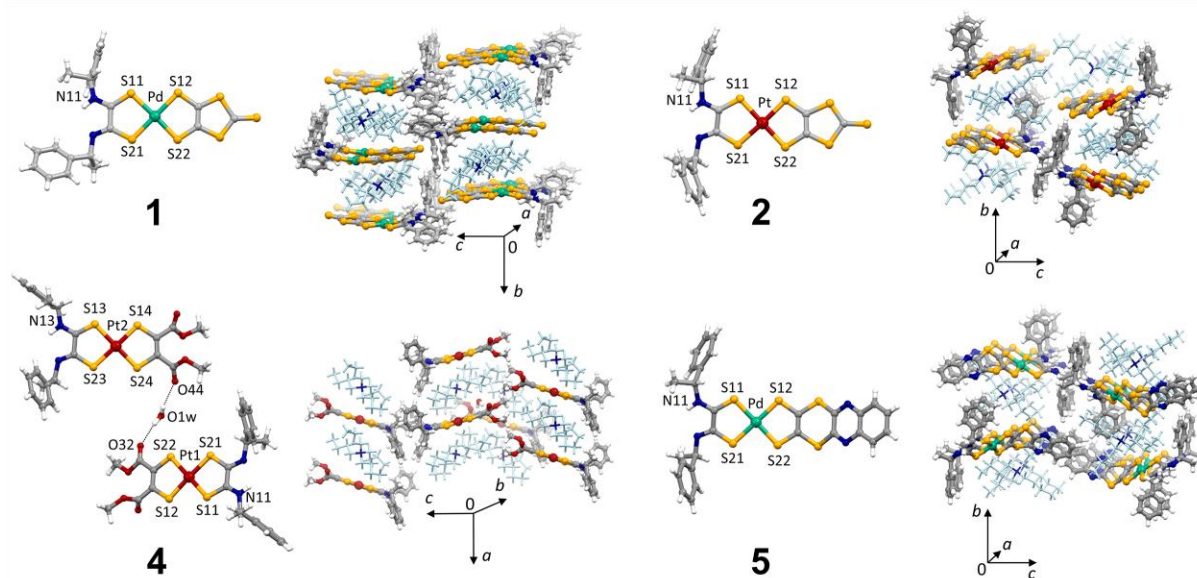
Figure 2. Molecular structures and crystal packing of compounds **1**, **2**, **4** and **5**. The Bu_4N^+ cations are depicted in light blue.

In all of the structures, the hydrogen atoms of the Bu_4N^+ cation interact with the sulphur atoms of the dithiolate ligand, see Figure 2. Indeed, according to DFT calculations, the dithiolate ligand exhibits the higher tendency to act as a nucleophilic site, since the electron density is mostly located on its C_2S_2 system as discussed further in the text. This observation points to the CH···S interactions as partly responsible of the crystal packing.

Optical properties and DFT calculations

The electronic absorption spectra of **1–6** in DMF solution are characterized by two main bands: one broad medium intense peak in the 525-606 nm range with a more or less resolved shoulder at higher frequency and a quite intense absorption band below 400 nm (Figure 3 and Figure S1). Similarly to what observed for **6**,[20a] upon addition of HCl, the color of the solutions changes and the lowest absorption band disappears while a new one is formed at higher wavelengths for a 1:1 molar ratio between HCl and the complexes, Table 1. The transformation can be reversed upon NH$_3$ addition, which allows the recovery of the original spectra when a 1:1 molar ratio, with respect to the protonated species, is reached. Figure 3 shows the spectra recorded from DMF solutions for **3** and **4**, as representative compounds.

In a second experiment, we have selected Ag$^+$ as a different type of electrophile than H$^+$. Indeed, in acidic conditions, the complex molecule is likely to be protonated on the nitrogen atom of the L1 ligand, thus promoting the formation of a double hydrogen bond with the chloride anions (see below). On the other hand, a soft metal such as Ag$^+$ is expected to interact with the sulphur atoms and even the metal of the coordination plane, providing a different perturbation of the frontier MOs mainly responsible of the optical properties. Treatment of **1-6** in DMF solutions with increasing amounts of silver trifluoromethanesulfonate (AgOTf) produces a change of the absorption spectra, with a blue shift of the peak in the visible region. The presence of well-defined isosbestic points suggests the formation of an equilibrium reaction between the complexes and a new absorbing species. By plotting Absorbances at λ_{max} versus increasing AgOTf amounts, a 1:2 ratio between the reagents has been determined. Removal of silver ions, for example upon HCl addition, allows the recovery of the protonated complexes as shown in Figure 4a for **6** as representative example (see also Figures S2 for **1** and **5** and S3 for **3**)
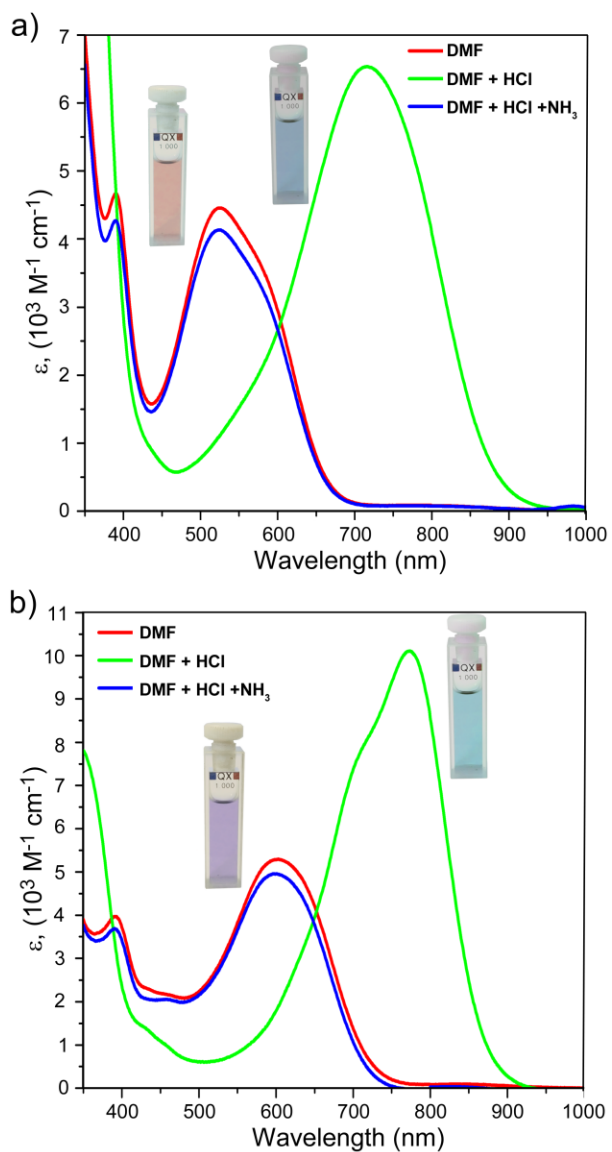
Figure 3. Electronic Spectra of **3** (above) and **4** (below) in DMF (blue), DMF+HCl (green) and DMF+HCl+NH$_3$, (red). Cuvettes containing solutions of **3** and **4** in DMF and in DMF+HCl and placed in proximity of related absorbance maxima, are included to show the color changes.

Complex	λmax	λmax	μβλ[d]	μβλ(HCl)[d,e]	NLO	Kurtz-

	(nm)[a] [b]	(nm)[c] [b]	(10^{-48}) esu	(10^{-48}) esu	(PMMA) χ^{33}(pm/V)	Perry[f]
1	525 [15.7]	747 [6.7]	−590	−2210	5.34±1.06	< detection limit
2	543 [9.6]	781 [9.6]	−1020	−2560	n.a.	< detection limit
3	525 [4.0]	715 [5.7]	−390	−2210	2.02±0.40	0.2
4	558 [5.5]	764 [11.1]	−480	−3120	1.32±0.26	0.5
5	550 [5.5]	773 [5.8]	−615	−1970	n.a.	< detection limit
6	606 [7.8]	814 [12.4]	−735	−298 0	n.a.	< detection limit

[a] DMF; [b] ε x10^3 (M^{-1} cm^{-1}); [c] DMF+HCl; [d] $CHCl_3$; [e] HCl vapour exposure; [f] efficiency ratio = intensity of complex/intensity of urea standard.

Table 1. Linear and non-linear optical properties of **1-6** complexes.

Thus, this species is likely a 1:2 adduct between the complexes and AgOTf. Despite we were unable to isolate these adducts in the solid state, we have performed DTF calculations in order to propose a reasonable structure in the presence of 2 equivalents of silver trifluoromethanesulfonate, Figures 4b, S4-S8 and Table S2 and S3. During the optimization, two molecular geometries were identified for the silver adduct, which differ by 4.9 kJ/mol. In the first optimized geometry, the silver cations are positioned above and below the coordination plane and interact in different ways with the coordination moiety. In particular, one Ag^+ lies above the Pt atom and exhibits a linear geometry with the oxygen atom of the $CF_3SO_3^-$ anion, whereas the second Ag^+ interacts with a sulphur atom of quinoxdt and with an oxygen atom of the second trifluoromethanesulfonate anion. In the second, and most stable geometry, the two AgOTf moieties are interacting more symmetrically with the coordination plane. Also, in this case the two Ag^+ are above and below the coordination plane, but both cations exhibit a linear coordination geometry with the oxygen atom of the $CF_3SO_3^-$ anion and the sulphur atoms of the coordination plane. For this geometry the Ag···Pt distances are greater than 3 Å.
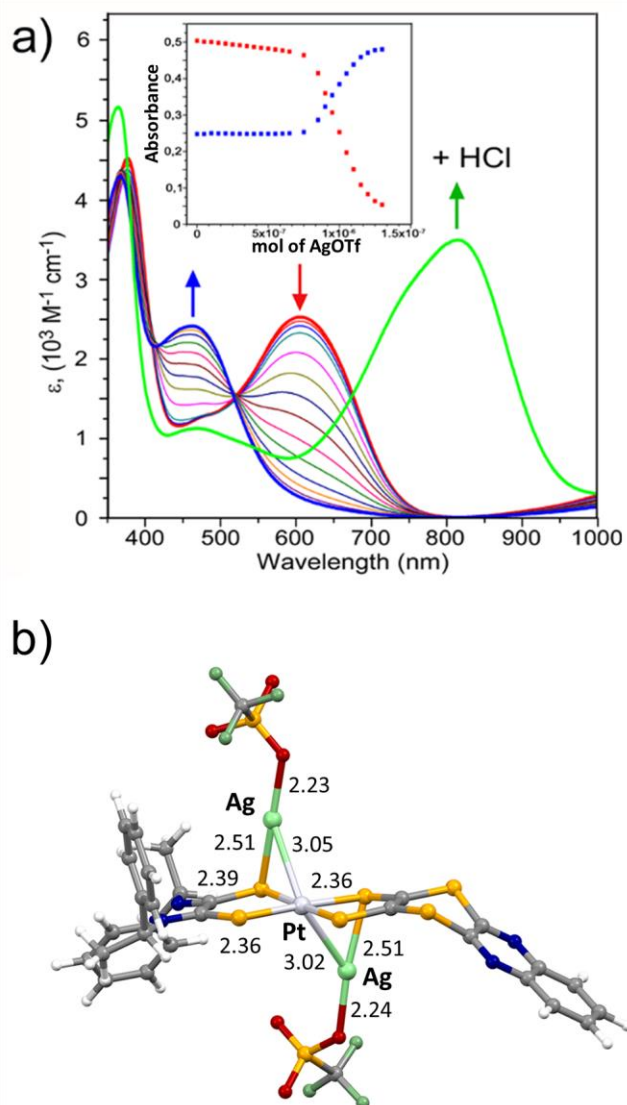
Figure 4. a) UV-Vis-NIR spectra of silver titration of complex **6** in DMF solution (conc = $1 \cdot 10^{-4}$ M); b) DFT optimized geometry of **6a·2AgOTf** (geometry **2**). B3lyp/6-31+G(d)_SDD with pseudo potential on Pt (MWB60) and Ag (MWB28) with the PCM method (dimethylformamide). Relevant bond distances (Å) are indicated.

The molecular geometry of **6·2AgOTf** is in agreement with the structural features of a similar system, namely [Pt(i-Pr$_2$pipdt)(quinoxdt)]·2AgOTf (where i-Pr$_2$pipdt = 1,4-di-isopropyl-piperazine-2,3-dithione),[47] previously reported. The computed optical properties are also in

agreement with the experimental results obtained on similar dithiolato-containing complexes treated with soft cation such as Au+ and Ag+.[47-49]
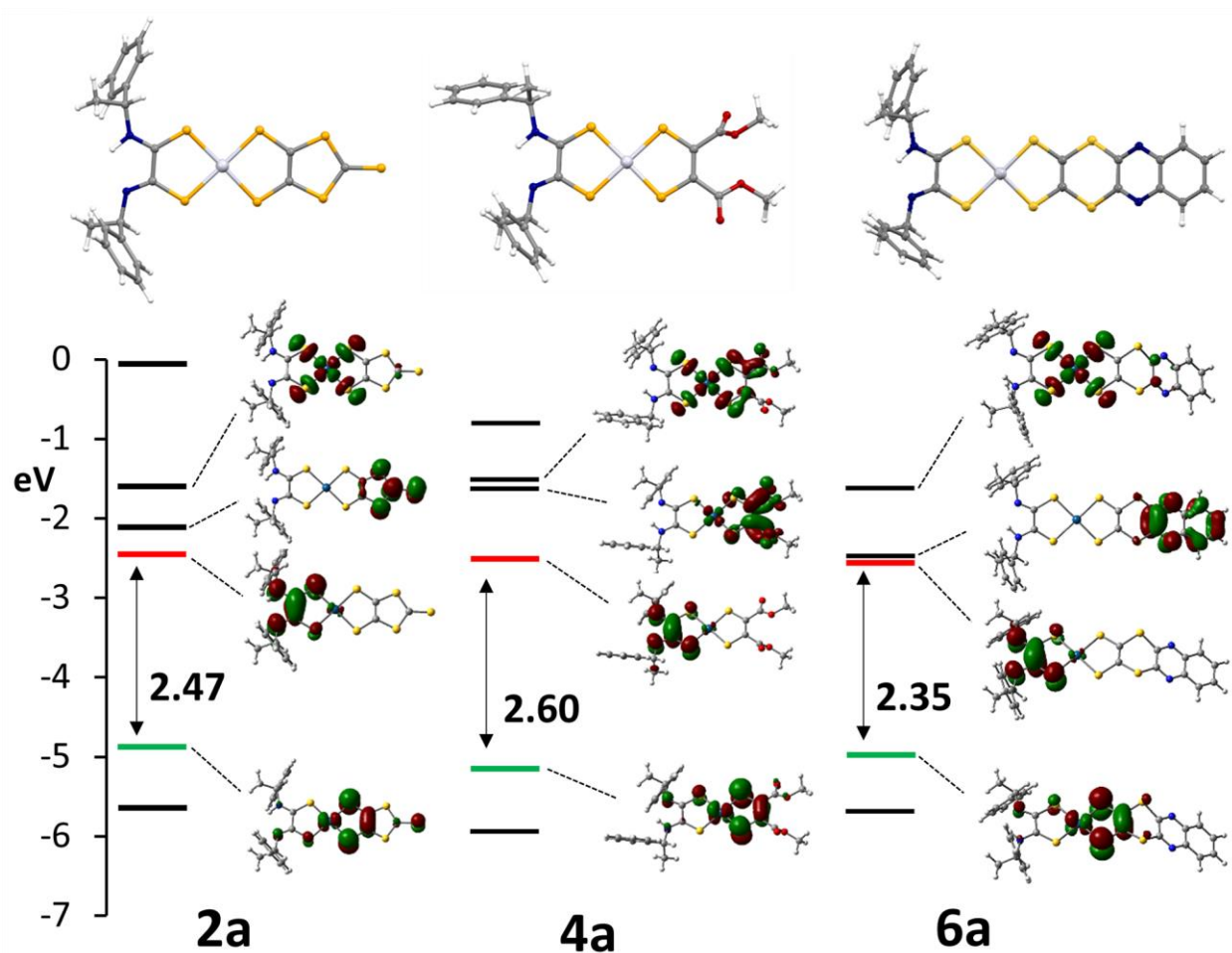
Figure 5. Energy levels and Kohn-Sham MOs for **2a**, **4a**, and **6a**. The calculation were performed at the B3LYP/6-31+G(d)_SDD level with the PCM method in N,N-dimethylformamide. HOMO green bar, LUMO red bar, energy gap in eV.

The electronic structures of the anionic complexes under discussion [Pd/Pt(L1)(L2)]$^-$ (**1a-6a**) were investigated by means of DFT methods and by taking into account the solvent (DMF) with the polarizable continuum method (PCM). The analysis of the frontier MOs shows that in all

complexes, the HOMO and LUMO are both formed from the out-of-plane antisymmetric interactions between the metal orbital and a ligand based C2S2 orbital (Figure 5 and Figures S9-S13). More specifically, the HOMO is mainly localized on the dithiolate system, whereas the LUMO is mainly localized on the dithio-oxamidate fragment, in agreement with previous findings for similar systems.[10,11,13,20,47,50]
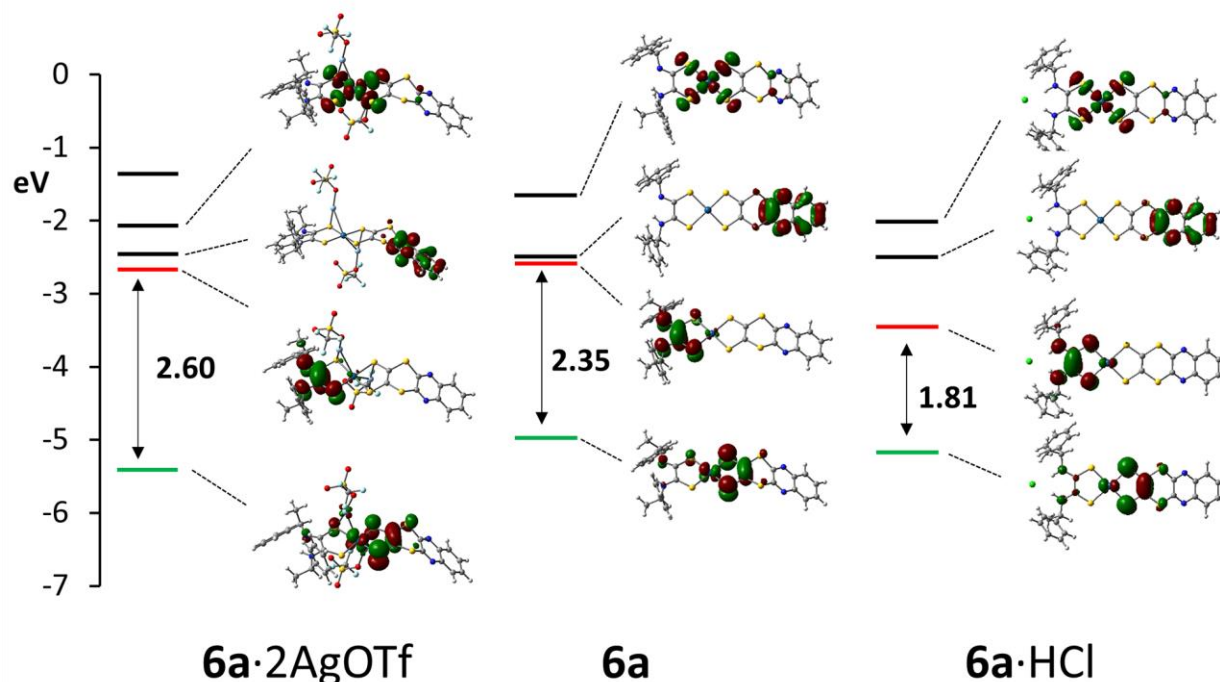
Figure 6. Energy levels and Kohn-Sham MOs for the adducts **6a**·2AgOTf (geometry **2**) (left), **6a**·(middle), and **6a**·HCl (right). The calculations were performed at the B3LYP/6-31+G(d)_SDD level with the PCM method in N,N-dimethylformamide. HOMO green bar, LUMO red bar, energy gap in eV.

The slightly nonsymmetric shape of the HOMO and LUMO reflects the presence of a hydrogen atom on only one of the thioamido group of the L1 ligand. The HOMO-LUMO gap varies little among the set of investigated complexes (2.35-2.60 eV) and, according to TD-DFT calculations, there is a good agreement between the calculated and experimental visible spectra for all of the compounds (Figure S14). The low energy absorption band can be associated almost exclusively

to an HOMO→LUMO transition (Tables S4-S8). Despite the donor ligands L2 have different molecular structures, the HOMO is mainly localized on the C2S2 moiety, thus resulting in similar electro-donor property during the charge-transfer transition. Moreover, by a comparison of the LUMO and LUMO+1 orbitals in the investigated systems, it appears that the presence of the quinoxdt ligand confers a significant stabilization to the LUMO+1. This latter MO is in fact located on the peripheral part of the quinoxdt moiety (anions **5a** and **6a**), and it is very close in energy to the LUMO. The computations were also performed on adducts formed by the complex molecules in presence of HCl (**1**·HCl, **2**·HCl, **4**·HCl), in order to describe the modulation of the absorption spectra as a function of the HCl addition. Previous studies by Campagna, Lanza, and co-workers,[51] showed that platinum homoleptic complexes coordinated to N,N′-dialkyldithio-oxamidate ligands form tight-contact ion pairs in presence of HX (X = Cl, Br, I), where the N··H··X interactions play a crucial role in stabilizing the ion-pair specie. Strong interactions between the N-H functions and the chloride counterion forming tight contact ion-paired complexes have been also observed in the 1,2- diamine system of oxalic amidines, that can be considered as bifunctional ligands capable of coupled cation/anion coordination.[52]

Similarly, in **1-6**, the most favourable protonation site is the nitrogen atom of L1, since a double N-H···Cl hydrogen bond can be formed (Figures S15-S17). This results in a more symmetrical shape of the MOs which confers a significant stabilization to the LUMO and consequently a decrease in the HOMO-LUMO energy gap, Figure 6. According to the TD-DFT calculations (Figure S18, Tables S9-S11), the presence of one equivalent of HCl per complex molecule, promotes a red shift of the low energy absorption band of more than 100 nm. As described above, we also investigated the influence of a Lewis acid, such as the silver cation, on the electronic feature of the system having the platinum and the quinoxaline ligand (compound **6**), where the silver ion interacts with both sides of the coordination plane. The interaction with the silver cation promotes a HOMO stabilization and a consequent increase of the HOMO-LUMO

gap (see Figure 6) leading to a blue shift of the low energy band of more than 100 nm. This agrees with what previously found for [Pt(i-Pr$_2$pipdt)(quinoxdt)] 2AgOTf.[47]

For the sake of completeness, the computations were also performed in the gas-phase for **2a**, **4a**, **6a** and **6a**·2AgOTf, Figures S19-S22. The gas-phase systems present a smaller HOMO-LUMO energy gap than the computations performed with a continuous solvent model, hence the experimental absorption properties are not satisfactorily modelled by the gas-phase computations.

Photoluminescence Studies

Remarkably, **5** exhibits switchable proton-dependent photoluminescence (PL) at room temperature in solution upon irradiation in the visible region at 450 nm (Figure 7 a and S23). Similar properties were previously observed for **6**.[20a] In **5** the emission color changes from visible red (λ_{max} = 670 nm) to yellow-green (λ_{max} = 573 nm) region upon the addition of a stoichiometric amount of HCl, as evidenced by the color coordinates in the CIE (Commission Internationale de l'Éclairage) chromaticity space shown in Figure 7b and Figure S26. This evident emission color change is attributed to the formation of a tight contact ion pair N··H··Cl which significantly affects the energy of the levels involved in the emission, as previously observed and discussed for **6** (Figure 6).[20a] Importantly, the subsequent addition of NH$_3$ totally quenches the green band and restores the initial conditions. Notably, an increase of about 20% of the integrated emission intensity is observed in basic conditions (approximately 4/1 [NH$_3$]/[HCl] ratio) with respect to the original state. This effect may be ascribed to the complete removal of residual water or acidic impurities in the solvent, which can interact with the basic sites of the molecule in the absence of the stabilization effect of the halogenide, resulting in emission quenching.

As already observed for **6**,[20] the emission is highly dependent on the excitation wavelength and it can be only triggered when irradiating at short wavelengths (Figure S23) while no emission is observed when exciting the HOMO-LUMO transition corresponding to the lowest absorption band. This peculiar behavior points out a break of the Kasha's rule, that is, radiative decay that occurs from excited states higher than the lowest excited state (associated to the LUMO).[23,53,54] This means that the typical relaxation from excited high-energy states through nonradiative internal conversion (IC) to the first excited state is unusually unfavored. An explanation for this phenomenon is associated to a strong intraligand charge-transfer (ILCT) character of the radiative decay process. In fact, emission originates from transitions between an upper state involving orbitals of the ligand periphery localized on the quinoxaline moiety (LUMO+1) to a ground state associated to the dithiolate core with some metal contribution (see the HOMO features in Figure 6) as recently supported by femtosecond UV−vis transient absorption spectroscopy studies.[20b] According to the DFT-calculated sequence of MOs, the poor spatial overlap between the superior Quinoxdt-based (LUMO+1) emissive state and the vicinal energy states (related to the LUMO) would slow down the LUMO+1→LUMO IC mechanism to the point that direct radiative decay LUMO+1 → HOMO becomes competitive, accounting for the observed anti-Kasha behaviour (Figure 7d). The difference in the emission wavelength between **5** (λ_{max} = 670 nm) and **6** (λ_{max} = 720 nm) is qualitatively in agreement with the increase of the energy gap between the LUMO+1 and the HOMO orbitals as evidenced by DFT calculations (Figures S9-10).
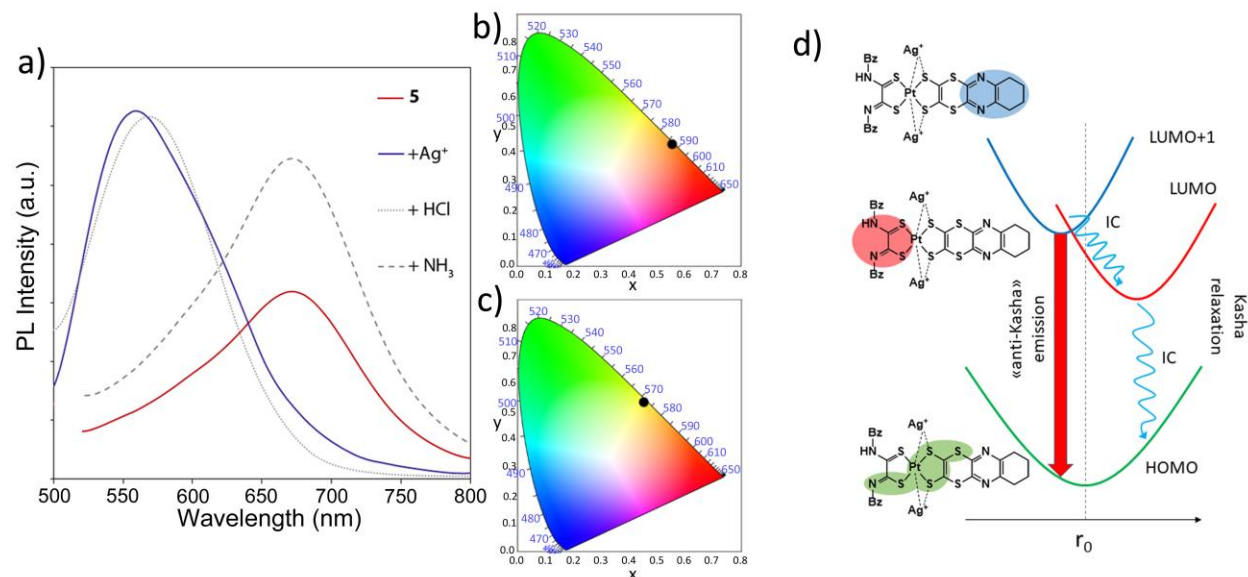
Figure 7. a). Emission spectra of **5** in DMF solution (red) and upon successive additions of 2 equivalents of AgOTf (blue), excess HCl (grey dotted line) and excess NH_3 (grey dashed line). Excitation wavelength was 450 nm. CIE1931 chromaticity diagrams are also shown for b) **5** and c) its silver adduct. d) Scheme of the energy levels and decay pathways for the silver adducts of **6**. The straight red arrow indicates radiative decay, the curved blue arrows represent nonradiative relaxation through internal conversion (IC).

The emission color of **5** and **6** notably changes upon addition of HCl and AgOTf. As shown in Figure 6 for **6**, upon acid addition, the interaction of a proton with the dithiooxamidate MBA-dto ligand does not change the sequence of MOs but increases the LUMO+1-HOMO gap mainly as a result of the stabilization of the HOMO, accounting for the blue shift of the observed emission, that still preserves the apparent anti-Kasha behavior. Remarkably, AgOTf addition induces a considerable blue shift of the emission of over 100 nm (λ_{max} = 559 nm). The maximum PL intensity is reached in the presence of 2 equivalents of Ag^+, in agreement with observations made with absorption experiments (Figure 4a) and further suggesting the formation of a 1:2 adduct with Ag^+. The preservation of the PL properties in the presence of Ag^+ noticeably deviates from

the behaviour previously observed[47] for the analogous complex [Pt(Pr$_2$pipdt)(quinoxdt)] where the silver adduct formation quenches the emission. This phenomenon was ascribed to a change in the nature of the involved energy levels, where the formerly emissive quinoxdt-based LUMO+1 changed to a metal – sulphur orbital with antibonding character in presence of silver.[47] Instead, in **6** the overall sequence of MOs is not affected by the interaction with Ag$^+$. As a consequence, the observed blue shift is consistent with the increase of the energy gap between the involved energy states (Figure 7d and S24). Interestingly, addition of HCl to the adduct solution induces a further change of the emission spectral range which shifts to 573 nm reflecting the properties observed upon protonation of the L1 moiety for the complex in the free form. The sequential addition of excess ammonia restores the initial properties of the free complex likely as a result of the dissociation of the silver adduct by the removal of Ag$^+$ after reaction with chloride or ammonia.

5 and **6** represent rather rare cases where the emission color can be reversibly tuned by different stimuli such as pH and the presence of metal ions. This is realized thanks to the combined synergy between ligand L1, able to react with protons, and the quinoxdt L2 ligand, which can establish strong interactions with metal ions and gives rise to emission properties that are unique among the class of Pt and Pd dithione-dithiolate complexes. It is worth noting that the change of the emission color is particularly significant, going from orange red (CIE chromaticity coordinates [0.53, 0.45], Figure 7b) for the free form to yellow-green (CIE coordinates [0.45, 0.53], Figure 7c) for the silver adduct or in the presence of HCl (CIE coordinates [0.45, 0.53]), Figure S25 and S26). This property, which combines with the color change related to the variation of the absorption profiles, could be useful for the development of molecule-based sensors which can be completely restored after usage.

NLO properties

As predictable, in addition to the described LO properties, these complexes exhibit proton switchable second order NLO properties. The NLO switches in solution are commonly studied by the Hyper-Rayleigh Scattering (HRS) technique working at 1064 nm incident wavelength which, however, suffers the limitation of possible overestimation of the value of the quadratic hyperpolarizability due to resonance. To achieve more reliable data, the EFISH (electric-field-induced second-harmonic generation) technique was employed to determine the second order NLO response of the molecular chromophores **1-5** in $CHCl_3$ solutions, working at non-resonant 1907 nm incident wavelength. From these measurements, $\mu\beta_\lambda$ can be obtained, where μ is the ground state dipole moment, β_λ is the projection along the dipole moment axis of the vectorial component β_{VEC} of the tensorial quadratic hyperpolarizability and λ is the fundamental wavelength of the incident photons (see details in Experimental Section). In fact, the EFISH technique can be applied also for the determination of the second order NLO response of ionic species by working in a solvent of a low dielectric constant such as $CHCl_3$, which favors ion pairing. Remarkably, it is found that $\mu\beta_{1907}$ value increases on protonation (see Table 1) by a factor ranging from 2.5 (for **2**) to 6.5 (for **4**). After NH_3 addition, absorption spectra and $\mu\beta_\lambda$ values determined in solution suggest that the NLO-phores **1-5** are restored.

The negative sign of $\mu\beta_{1907}$ values is in agreement with a decrease of the dipolar moments of the excited states. A similar behaviour was reported for the Pt complex **6**[20] with an increase factor of $\mu\beta_{1907}$ value of 4.

SHG efficiency of crystalline powders was determined according to the Kurtz-Perry method at 1907 nm. Despite **1**, **2**, **4**, **5** and **6** crystallize in a non-centrosymmetric space group, only **3** and **4** produced a measurable SHG value (0.2 for **3** and 0.5 for **4**, by comparing the intensity with three urea standard). The efficiency ratio for **1**, **2** and **6** resulted at the background noise limit. These

results can be explained by taking into account that, while all the measured crystals belong to non-centrosymmetric point groups, **4** crystallizes in the polar *P*1 space group, and two independent complex molecules, with different orientations, are present in the asymmetric unit (see Figures S27-S29). Contrarily, **1-2** and **5-6** crystallize in the non-polar *P2₁2₁2₁* space group, which, although non-centrosymmetric, is unfavorable to a non-null SGH signal.

Composite thin films of **1**, **3** and **4** complexes in PMMA matrix were prepared as reported in the Experimental section. The UV-vis absorption spectra of **1**, **3** and **4** films before poling are shown in Figures S30-S32. They are characterized by a broad absorption band in the visible region at 512, 546 and 485 nm, respectively. This absorption band is related to the charge transfer transition from the donor (L2) to the acceptor (L1) ligand, as already observed for the **1**, **3** and **4** complexes in the DMF solution.

Second-order NLO properties of **1**, **3** and **4** thin films were induced by applying the corona-wire poling technique (see Experimental Section). In order to avoid degradation of the film and to increase the SHG signal as much as possible, an optimization of the temperature and applied electric field during the poling was necessary for each film. The corona-wire poling dynamics of **1**, **3** and **4** thin films is shown in Figures 8, S33 and S34, respectively. The best conditions were the following: 70 °C and 10 kV for **1** and **3**, and 80 °C and 10 kV for **4**. When analyzing the poling dynamics of the three films a general behavior can be observed. The SHG signal is negligible at room temperature and increases as the temperature is increased close to the glass-transition temperature (T_g) of PMMA (86.5°C) and the electric field is applied (10 kV), reaching its maximum value in about 60–90 min. This is due to the decrease of the viscosity of the PMMA matrix near the T_g, which allowed an easier orientation of the NLO chromophores. After the SHG signal reached the plateau, the temperature was decreased to room temperature, "freezing" the orientation of the chromophores inside the polymeric matrix, then the dry-box is opened and the electric field is turned off. During the cooling process and after the removal of

the electric field, we did not observe any marked decrease of the SHG signal suggesting no appreciable reorientation of the chromophores within the polymeric matrix.

Table 2. Coefficients of the second-order susceptibility tensor $\chi^{ij(2)}$ for **1**, **3** and **4** films.

Film	$\chi 33^{(2)}$(pm/V)	$\chi 31^{(2)}$(pm/V)	$\chi 15^{(2)}$(pm/V)
1	5.34 ± 1.06	1.62 ± 0.32	1.56 ± 0.31
3	2.02 ± 0.40	0.70 ± 0.14	0.62 ± 0.12
4	1.32 ± 0.26	0.46 ± 0.09	0.40 ± 0.08

Absorption spectra of the **1**, **3** and **4** films recorded after poling (Figures S23-S25) show that the broad absorption band in the visible region of each film remains unchanged in shape, but the intensity decreases compared to that recorded before poling. This phenomenon is the so-called dichroic effect, due to the partial orientation of molecules along the direction of the electric poling field.[55,56] Moreover, no appreciable Stark shift[55,56] of the absorption peaks was observed after poling.
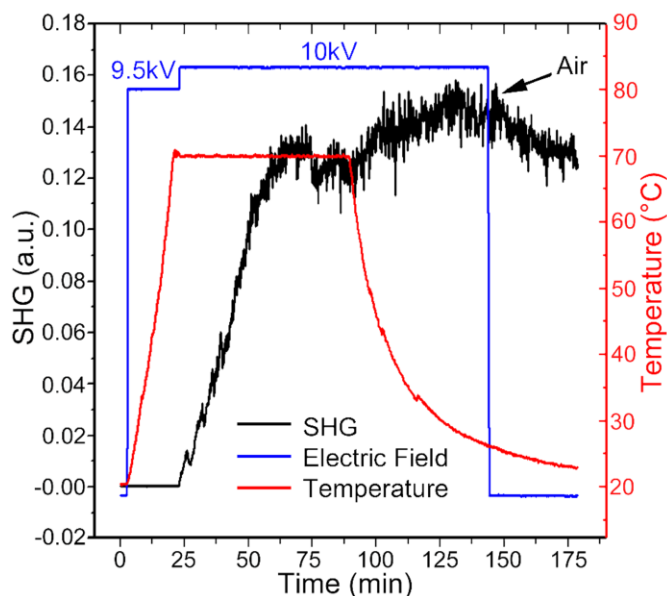
Figure 8. Corona-wire poling dynamics of **1** film.

By fitting the Maker fringe measurements, using the expressions expected for poled films with $C_{\infty v}$ symmetry,[44,57] the three nonzero coefficients of the second-order susceptibility tensor $\chi_{33}^{(2)}$, $\chi_{31}^{(2)}$ and $\chi_{15}^{(2)}$ for the poled **1**, **3** and **4** films were evaluated (Table 3). From the data in Table 3 we observe that the $\chi_{31}^{(2)}$ and $\chi_{15}^{(2)}$ components of each film are approximately equal to $\chi_{33}^{(2)} / 3$ within the experimental error; this is a result generally valid for poled thin film of push-pull type chromophores in which the charge transfer from the donor to the acceptor ligand is predominantly mono-dimensional. Moreover, the values of the components of the susceptibility tensor for **1** are higher than those obtained for **3** which in turn are higher of **4**, a behavior similar to what observed in solution. In addition, the susceptibility tensor for the film **1** is higher than the similar Pd(II) dithione/dithiolate complex in the PMMA matrix ($\chi_{33}^{(2)} = 1.86$ pm V^{-1}, $\chi_{31}^{(2)} = 0.24$ pmV^{-1} and $\chi_{15}^{(2)} = 0.20$ pmV^{-1}), reported in reference 58 although it should be noted that the values in Table 3 are affected by resonant enhancement owing to the non-zero absorption of the complexes at the 532 nm (second harmonic wavelength). Attempts to protonate the films with HCl vapors (as reported in the Experimental section) have given no change in the properties, probably due to the difficulty of the acid to penetrate into the polymeric matrix.

Conclusion

In this paper, we describe Donor-M-Acceptor systems designed to achieve switchable linear and nonlinear optical properties. The systems comprise metal-d^8-heteroleptic square-planar dithiolenes, namely Bu$_4$N[M^{II}(L1)(L2)] (M= Pd, Pt). L1 is the acceptor system consisting in the chiral (*R*)-(+)-α-methylbenzyl dithio-oxamidate, capable to undergo proton exchange. L2 is the donor dithiolate moiety, which varies whilst maintaining similar electrodonating capability of the

C2S2 moiety: dmit, in **1**(Pd)/**2**(Pt); ddmet in **3**(Pd)/**4**(Pt); quinoxdt in **5**(Pd)/**6**(Pt). **1-6** behave as proton and silver switchable linear chromophores. Indeed, they are characterized by a color change with a shift to lower energies of the CT peak for proton addition (acidochromes). On the opposite, when forming a 1:2 adduct with silver trifluoromethanesulphonate, they are accompanied by a shift of this peak to higher energies. The modulation of the visible absorption properties can be rationalized by taking into account: i) the stabilization of the LUMO as a consequence of the L1 protonation, and ii) a stabilization of the HOMO when a soft cation such as Ag^+ interacts with the metal-sulphurs coordination environment. These proton- and silver-switchable properties are thus realized thanks to the effective interplay of L1, capable to undergo proton exchange, and L2 capable to establish strong interactions with *soft*-metal ions. Moreover, their second-order NLO response is also proton switchable, resulting significantly increased for L1 protonation as a consequence of its increased acceptor behavior. In the bulk, satisfactory NLO response has been determined for **1**, **3** and **4** when embedded into PMMA poled matrix, and a measureable value of the SHG efficiency ratio was also determined for crystals of **4**. Remarkably, **5-6,** bearing a quinoxaline moiety, show anti-Kasha proton and silver tunable colored emission, unique among the class of Pt and Pd dithione-dithiolate complexes.

Thus, the bottom-up tailoring of heteroleptic metal-dithiolenes, performed by integrating specific functional groups in the ligands, has shown to be a versatile tool to improve their multifunctional capability to achieve a reversible response to external stimuli. This strategy can further promote the optimization of these and similar complexes for potential applications as self-indicating proton and silver titrants in non-aqueous solvents,[51] as well as molecular sensors and switches in optoelectronics.

Supporting Information paragraph.

Additional details of crystallographic data, UV–vis absorption spectral data, results from the DFT and TD-DFT calculations, photoluminescence, second-order non-linear optical properties.

Conflict of Interest Disclosure.

The authors declare no competing financial interest.

Present Addresses

† Salahuddin S. Attar, Department of Chemistry, Texas A&M University at Qatar (TAMUQ), P. O. Box 23874, Texas A&M Engineering Building, Education City, Doha (Qatar). ‼ Davide Espa, external collaborator at Dipartimento di Ingegneria Meccanica, Chimica e dei Materiali, Università di Cagliari, via Marengo 2, 09123 Cagliari (Italy). ‡ Paola Deplano, external collaborator at Dipartimento di Ingegneria Civile, Ambientale e Architettura, INSTM Research Unit, Università di Cagliari, via Marengo 2, 09123 Cagliari (Italy).

Author Contributions

The manuscript was written through contributions of all authors. All authors have given approval to the final version of the manuscript.

REFERENCES

(1) Sproules, S. and Wieghardt, K**.** Dithiolene radicals**:** Sulfur K-edge X-ray absorption spectroscopy and Harry's intuition. *Coord. Chem. Rev.*, **2011**, *255*, 837–860.

(2) Kusamoto, T. and Nishihara, H. Zero-, one- and two-dimensional bis(dithiolato)metal complexes with unique physical and chemical properties. *Coord. Chem. Rev.*, **2019**, *380*, 419–439.

(3) Kato, R. Conducting Metal Dithiolene Complexes: Structural and Electronic Properties, *Chem. Rev.*, **2004**, *104 (11)*, 5319−5346.

(4) Perochon, R.; Davidson, P.; Rouzière, S.; Camerel, F.; Piekara-Sady, L.; Guizouarn T. and Fourmigué, M. Probing magnetic interactions in columnar phases of a paramagnetic gold dithiolene complex. *J. Mater. Chem.*, **2011**, *21*, 1416−1422.

(5) Shirakawa, Y.; Takahashi, K.; Sato, H.; Hoshino, N.; Anetai, H.; Noro, S.-I.; Akutagawa T. and Nakamura, T. Hydrogen-Bonded Polyrotaxane Cation Structure in Nickel Dithiolate Anion Radical Salts: Ferromagnetic and Semiconducting Behavior Associated with Structural Phase Transition. *Chem. Eur.J.*, **2019**, *25*, 6920–6927.

(6) Islam, A.; Sugihara, H.; Hara, K.; Singh, L. P.; Katoh, R.; Yanagida, M.; Takahashi, Y.; Murata, S.; Arakawa, H. and Fujihashi, G. Dye Sensitization of Nanocrystalline Titanium Dioxide with Square Planar Platinum(II) Diimine Dithiolate Complexes. *Inorg. Chem.*, **2001**, *40*, 5371−5380.

(7) Linfoot, L.; Richardson, P.; McCall, K. L.; Durrant, J. R.; Morandeira A. and Robertson, N. A nickel-complex sensitiser for dye-sensitised solar cells. *Solar Energy*, **2011**, *85*, 1195−1203.

(8) Li, G.; Mark, M. F.; Lv, H.; McCamant D. W. and Eisenberg, R. Rhodamine-Platinum Diimine Dithiolate Complex Dyads as Efficient and Robust Photosensitizers for Light-Driven Aqueous Proton Reduction to Hydrogen. *J. Am. Chem. Soc.*, **2018**, *140 (7)*, 2575−2586.

(9) Pilia, L.; Pizzotti, M.; Tessore F. and Robertson, N. Nonlinear-optical properties of *α*-diiminedithiolato nickel(II) complexes enhanced by electron-withdrawing carboxyl groups. *Inorg. Chem.*, **2014**, *53*, 4517−4526.

(10) Espa, D.; Pilia, L.; Marchio, L.; Mercuri, M. L.; Serpe, A.; Barsella, A.; Fort, A.; Dalgleish, S. J.; Robertson N. and Deplano, P. Redox Switchable Chromophores based on Metal (Ni, Pd, Pt) Mixed-Ligand Dithiolene Complexes Showing Molecular Second-order NLO Activity. *Inorg. Chem.*, **2011**, *50 (6)*, 2058–2060.

(11) Espa, D.; Pilia, L.; Attar, S.; Serpe, A. and Deplano, P. Molecular Engineering of Heteroleptic Metal-Dithiolene Complexes with Optimized Second-order NLO Response. *Inorg. Chimica Acta*, **2018**, *470*, 295−302.

(12) a) Sobottka, S.; Nößler, M.; Ostericher, A. L.; Hermann, G.; Subat, N. Z.; Beerhues, J.; Behr-van der Meer, M.; Suntrup, L.; Albold, U.; Hohloch, S.; Tremblay, J. C.; and Sarkar, B. Tuning Pt II-Based Donor–Acceptor Systems through Ligand Design: Effects on Frontier Orbitals, Redox Potentials, UV/Vis/NIR Absorptions, Electrochromism, and Photocatalysis. *Chem. Eur. J.*, **2020**, *26*, 1314–1327; b) Mandapati, P.; Braun, J. D.; Lozada, I. B.; Williams, J. A. G.; and Herbert, D. E. Deep-Red Luminescence from Platinum(II) Complexes of N^N−^N Amido Ligands with Benzannulated N Heterocyclic Donor Arms. *Inorg. Chem.*, **2020**, *59*, 12504−12517; c) Durand, R. J.; Gauthier, S.; Achelle, S.; Kahlal, S.; Saillard, J.-Y.; Barsella, A.; Wojcik,

L.; Le Poul, N.; Robin-Le Guen, F. Incorporation of a platinum center in the pi-conjugated core of push–pull chromophores for nonlinear optics (NLO). *Dalton Trans.*, **2017**, *46*, 3059–3069; d) Nisic, F.; Cariati, E.; Colombo, A.; Dragonetti, C.; Fantacci, S.; Garoni, E.; Lucenti, E.; Righetto, S.; Roberto D.; and Williams, J. A. G. Tuning the dipolar second-order nonlinear optical properties of 5-π-delocalized-donor-1,3-di(2-pyridyl) benzenes, related cyclometallated platinum(II) complexes and methylated salts. *Dalton Trans.*, **2017**, *46*, 1179–1185; e) Yam, V. W.-W.; Law, A. S.-Y. Luminescent d8 metal complexes of platinum(II) and gold(III): From photophysics to photofunctional materials and probes. *Coord. Chem. Rev.*, **2020**, *414*, 213298−213307; f) Drosou, M.; Kamatsos, F.; Mitsopoulou, C. A. Recent advances in the mechanisms of the hydrogen evolution reaction by non-innocent sulfur-coordinating metal complexes. *Inorg. Chem. Front.*, **2020**, *7*, 37−71.

(13) Deplano, P.; Espa, D.; Pilia, L. "Recent Advances in the structure and properties of metal-dithiolene complexes" PATAI's Chemistry of Functional Groups, The Chemistry of Metal Enolates, Vol 2, Ch. 14, pp 515-545, Edited by J. Zabicky, J. Wiley& Sons Ltd, Chichester, **2018**.

(14) a) Zyss, J. Molecular Nonlinear Optics: Materials, Physics and Devices; Academic Press: Boston, **1994**; b) Colombo, A.; Nisic, F.; Dragonetti, C.; Marinotto, D.I.; Oliveri, P.; Righetto, S.; Lobello M. G. and De Angelis, F. Unexpectedly high second-order nonlinear optical properties of simple Ru and Pt alkynyl complexes as an analytical springboard for NLO-active polymer films. *Chem. Commun.*, **2014**, *50*, 7986−7989.

(15) Boixel, J.; Guerchais, V.; Le Bozec, H.; Jacquemin, D.; Amar, A.; Boucekkine, A.; Colombo, A.; Dragonetti, C.; Marinotto, D.; Roberto, D.; Righetto S. and De Angelis,

R. Second-Order NLO Switches from Molecules to Polymer Films Based on Photochromic Cyclometalated Platinum(II) Complexes. *J. Am. Chem. Soc.* **2014**, *136 (14)*, 5367−5375.

(16) Coe, B. J. Molecular Materials Possessing Switchable Quadratic Nonlinear Optical Properties, *Chem. Eur. J.*, **1999**, *5*, 2464−2471.

(17) B. Feringa, B. L. Feringa and W. R. Browne, Eds. Molecular Switches, 2nd ed.; Wiley-VCH: Weinheim, **2011**.

(18) Zhao, Y.; Ippolito, S. and Samorì, P. Functionalization of 2D Materials with Photosensitive Molecules: From Light-Responsive Hybrid Systems to Multifunctional Devices. *Adv. Optical Mater.,* **2019**, *7*, 1900286.

(19) Rosace, G.; Giuffrida, G.; Saitta, M.; Guglielmo, G.; Campagna, S. and Lanza, S. Luminescence Properties of Platinum(II) Dithiooxamide Compounds, *Inorg. Chem.* **1996**, *35*, 6816-6822; b) Nastasi, F.; Puntoriero, F.; Palmeri, N.; Cavallaro, S.; Campagna S. and Lanza S. Solid-state luminescence switching of platinum(II) dithiooxamide complexes in the presence of hydrogen halide and amine gases, *Chem. Commun.*, **2007**, 4740–4742.

(20) a) Attar, S.; Espa, D.; Artizzu, F.; Pilia, L.; Serpe, A.; Pizzotti, M.; Di Carlo, G.; Marchiò, L. and Deplano P. Optically Multiresponsive Heteroleptic Platinum-dithiolene Complex with Proton Switchable Properties. *Inorg. Chem.* **2017**, *56*, 6763−6767; b) M. Gazzetto, F. Artizzu, S. S. Attar, L. Marchiò, L. Pilia, E. J. Rohwer, T. Feurer, P. Deplano, and A. Cannizzo Anti-Kasha Conformational Photoisomerization of a Heteroleptic Dithiolene Metal Complex Revealed by Ultrafast Spectroscopy, *J. Phys. Chem. A*, **2020**, 124, *51*, 10687–10693.

(21) Lenoble, G.; Lacroix, P. G.; Daran, J. C.; Di Bella S. and Nakatani, K. Syntheses, Crystal Structures, and NLO Properties of New Chiral Inorganic Chromophores for Second-Harmonic Generation, *Inorg. Chem.*, **1998**, *37*, 2158−2165.

(22) Rivera, J. M.; Reyes, H.; Corte´s, A.; Santillan, R.; Lacroix, P. G.; Lepetit, C.; Nakatani K. and Farfán, N. Second-Harmonic Generation within the $P2_12_12_1$ Space Group, in a Series of Chiral (Salicylaldiminato)tin Schiff Base Complexes. *Chem. Mater.*, **2006**, *18*, 1174-1183.

(23) Kasha, M. Characterization of electronic transitions in complex molecules *Discuss. Faraday Soc.*, **1950**, *9*, 14−19.

(24) Hurd, R. N.; De La Mater G.; McElheny, G. C.; Turner, R. J.; Wallingford, V. H. Preparation of Dithiooxamide Derivatives. *J. Org. Chem.* **1961**, *26*, 3980−3987.

(25) Bruker (2012). SMART. Bruker AXS Inc., Madison, Wisconsin, USA.

(26) Krause, L.; Herbst-Irmer, R.; Sheldrick G.M. and Stalke, D. Comparison of silver and molybdenum microfocus X-ray sources for single-crystal structure determination, *J. Appl. Cryst.* **2015**, *48*, 3−10.

(27) Burla, M. C.; Caliandro, R.; Camalli, M.; Carrozzini, B.; Cascarano, G. L.; Giacovazzo, C.; Mallamo, M.; Mazzone, A.; Polidori, G.; Spagna, R. SIR2011: A new package for crystal structure determination and refinement, *J. Appl. Cryst.* **2012**, *45*, 357–361.

(28) Sheldrick G. M. SHELXT – Integrated space-group and crystal-structure determination. *Acta Cryst. Section A* **2015**, *71*, 3−8.

(29) Sheldrick, G.M. Crystal structure refinement with *SHELXL* (**2015**) *Acta Cryst. C71*, 3-8.

(30) Macrae, C. F.; Edgington, P. R.; McCabe, P.; Pidcock, E.; Shields, G. P.; Taylor, R.; Towler M. and van de Streek, J. Mercury: Visualization and Analysis of Crystal Structures. *J. Appl. Cryst.* **2006**, *39*, 453−457

(31) Parr, R. G.; Yang, W. Density-Functional Theory of Atoms and Molecules; Oxford University Press: New York, **1989**.

(32) Gaussian 16, Frisch, M. J.; Trucks, G. W.; Schlegel, H. B.; Scuseria, G. E.; Robb, M. A.; Cheeseman, J. R.; Scalmani, G.; Barone, V.; Petersson, G. A.; Nakatsuji, H.; Li, X.; Caricato, M.; Marenich, A.V.; Bloino, J.; Janesko, B.G.; Gomperts, R.; Mennucci, B.; Hratchian, H.P.; Ortiz, J.V.; Izmaylov, A.F.; Sonnenberg, J.L.; Williams-Young, D.; Ding, F.; Lipparini, F.; Egidi, F.; Goings, J.; Peng, B.; Petrone, A.; Henderson, T.; Ranasinghe, D.; Zakrzewski, V.G.; Gao, J.; Rega, N.; Zheng, G.; Liang, W.; Hada, M.; Ehara, M.; Toyota, K.; Fukuda, R.; Hasegawa, J.; Ishida, M.; Nakajima, T.; Honda, Y.; Kitao, O.; Nakai, H.; Vreven, T.; Throssell, K.; Montgomery Jr., J.A.; Peralta, J.E.; Ogliaro, F.; Bearpark, M.J.; Heyd, J.J.; Brothers, E.N.; Kudin, K.N.; Staroverov, V.N.; Keith, T.A.; Kobayashi, R.; Normand, J.; Raghavachari, K.; Rendell, A.P.; Burant, J.C.; Iyengar, S.S.; Tomasi, J.; Cossi, M.; Millam, J.M.; Klene, M.; Adamo, C.; Cammi, R.; Ochterski, J.W.; Martin, R.L.; Morokuma, K.; Farkas, O.; Foresman, J.B. and Fox, D.J. Gaussian, Inc., Wallingford CT, **2016**.

(33) Becke, D. Density-functional exchange-energy approximation with correct asymptotic behavior, Physical Review A: Atomic, Molecular, and Optical Physics **1988**, *38[6]*, 3098−3100.

(34) Becke, D. Density-functional thermochemistry. III. The role of exact exchange, *J. Chem. Phys.* **1993**, *98 (7)*, 5648−5652.

(35) Ditchfield, R. Hehre, W. J. and Pople, J. A. Self-Consistent Molecular-Orbital Methods. IX. An Extended Gaussian-Type Basis for Molecular-Orbital Studies of Organic Molecules, *J. Chem. Phys.* **1971**, *54*, 724.

(36) Rassolov, V. A.; Ratner, M. A.; Pople, J. A.; Redfern, P. C. and Curtiss, L. A. 6-31G* basis set for third-row atoms, *J. Comp. Chem.* **2001**, *22*, 976.

(37) Fuentealba, P.; Preuss, H.; Stoll, H. and Szentpaly, L. v. A proper account of core-polarization with pseudopotentials: single valence-electron alkali compounds, *Chem. Phys. Lett.* **1982**, *89*, 418.

(38) Cao, X. Y. and Dolg, M. Segmented contraction scheme for small core lanthanide pseudopotential basis sets, *J. Mol. Struct. (Theochem)* **2002**, 581, 139−147.

(39) Schwerdtfeger, P.; Dolg, M.; Schwarz, W. H. E.; Bowmaker, G. A. and Boyd, P. D. W. Relativistic effects in gold chemistry. I. Diatomic gold compounds, *J. Chem. Phys.* **1989**, *91*, 1762.

(40) Mennucci B. and Tomasi, J. Continuum solvation models: A new approach to the problem of solute's charge distribution and cavity boundaries, *J. Chem. Phys. J. Chem. Phys.* **1997**, *106*, 5151-5158.

(41) Casida, M. E.; Jamorski, C.; Casida, K. C.; Salahub, D. R. Molecular excitation energies to high-lying bound states from time-dependent density-functional response theory: Characterization and correction of the time-

dependent local density approximation ionization threshold, *J. Chem. Phys.* **1998**, *108*, 4439-4449.

(42) Stratmann, R. E.; Scuseria, G. E.; Frisch, M. J. An efficient implementation of time-dependent density-functional theory for the calculation of excitation energies of large molecules, *J. Chem. Phys.* **1998**, *109*, 8218-8224.

(43) Gorelsky, S. I. AOMix: Program for Molecular Orbital Analysis, http://www.sg-chem.net/, version 6.52, **2011**.

(44) Herman W. N. and Hayden L. M., Maker fringes revisited: second-harmonic generation from birefringent or absorbing materials, *J. Opt. Soc. Am. B*, **1995**, *12*, 416-427.

(45) Maker, P. D.; Terhune, R. W.; Nisenoff M. and Savage, C. M. Pseudosymmetric Features and Nonlinear Optical Properties of Potassium Titanyl Phosphate Crystals, *Phys. Rev. Lett.*, **1962**, *8*, 21-22.

(46) Jerphagnon, J. and Kurtz, S. K. Maker Fringes: A Detailed Comparison of Theory and Experiment for Isotropic and Uniaxial Crystals, *J. Appl. Phys*., **1970**, *41*, 1667-1681

(47) Attar, S.; Artizzu, F.; Marchiò, L.; Espa, D.; Pilia, L.; Casula, M. F.; Serpe, A.; Pizzotti, M.; Orbelli-Biroli, A. and Deplano, P. Uncommon Optical Properties and Silver-ResponsiveTurn-Off/On Luminescence in a Pt^{II} Heteroleptic Dithiolene Complex. *Chem. Eur. J.,* **2018**, *24*,10503–10512.

(48) Juliá, F.; Jones P. and González-Herrero, P. Synthesis and Photophysical Properties of Cyclometalated Platinum(II) 1,2-Benzenedithiolate Complexes and Heterometallic

Derivatives Obtained from the Addition of $[Au(PCy_3)]^+$ Units, *Inorg. Chem.*, **2012**, *51*, 5037.

(49) Moussa, J.; Chamoreau, L.M.; Gullo, M.P.; Degli Esposti, A.; Barbieri, A. and Amouri, H. Induced phosphorescence from Pt → Ag and Ag(i)···Ag(i) metallophilic interactions in benzenedithiolatodiimine-Pt_2/Ag_2 clusters: a combined experimental and theoretical investigatio*n Dalton Trans*., **2016**, *45*, 2906.

(50) Pilia, L.; Espa, D.; Barsella, A.; Fort, A.; Makedonas, C.; Marchiò, L.; Mercuri, M. L.; Serpe, A.; Mitsopoulou, C. A., Deplano, P. Combined Experimental and Theoretical Study on Redox-Active d^8 Metal Dithione-Dithiolato Complexes Showing Molecular Second-Order Nonlinear Optical Activity, *Inorg. Chem.* **2011**, *50*, 10015−10027.

(51) a) Giannetto, A.; Puntoriero, F.; Barattucci, A.; Lanza, S.; Campagna, S. Tight-contact ion pairs involving Pt(II) dithiooxamide complexes: The acid-base reactions between hydrohalogenated ion-paired complexes and pyridine. *Inorg. Chem.* **2009**, *48*, 10397−10404; b) A. Giannetto, M. Cordaro, S. Campagna, S. Lanza, Metal Complexes as Self-Indicating Titrants for Acid−Base Reactions in Chloroform, *Inorg. Chem.* **2018**, *57*, 2175−2183.

(52) Rau, S.; Böttcher, L.; Schebesta, S.; Stollenz, M.; Görls, H.; Waltherit, D. Simultaneous Cation/Anion Coordination by Bifunctional 1,2-Diimine/1,2-Diamine Type Ligands: Synthesis, Structures, and Properties of Tight Ion Pair Complexes of Ruthenium and Iron. *Eur. J. Inorg. Chem.*, **2002**, 2800−2809.

(53) Tseng, H.-W.; Shen, J.-Y.; Kuo, T.-Y.; Tu, T.-S.; Chen, Y.-A., Demchenko A. P. and Chou, P.-T. Excited-state intramolecular proton transfer reaction demonstrating anti-Kasha behavior, *Chem. Sci.*, **2016**, *7*, 655−665.

(54) a) Scuppa, S.; Orian, L.; Donoli, A.; Santi S. and Meneghetti, M. Anti-Kasha's rule fluorescence emission in (2-ferrocenyl)indene generated by a twisted intramolecular charge-transfer (TICT) process, *J. Phys. Chem. A*, **2011**, *115*, 8344−8349; b) Daniel Escudero and Walter Thiel; Exploring the Triplet Excited State Potential Energy Surfaces of a Cyclometalated Pt(II) Complex: Is There Non-Kasha Emissive Behavior? *Inorg. Chem.*, **2014**, *53*, 11015−11019.

(55) Page, R. H.; Jurich, M. C.; Reck, B.; Sen, A.; Twieg, R. J.; Swalen, J. D.; Bjorklund G. C. and Wilson, C. G. Electrochromic and optical waveguide studies of corona-poled electro-optic polymer films, *J. Opt. Soc. Am. B*, **1990**, *7*, 1239–1250.

(56) Mortazavi, M. A.; Knoesen, A.; Kowel, S. T.; Higgins B. G. and Dienes A., Second-harmonic generation and absorption studies of polymer–dye films oriented by corona-onset poling at elevated temperatures, *J. Opt. Soc. Am. B*, **1989**, *6*, 733–741.

(57) Marinotto, D.; Castagna, R.; Righetto, S.; Dragonetti, C.; Colombo, A.; Bertarelli, C.; Garbugli M. and Lanzani, G. Photoswitching of the Second Harmonic Generation from Poled Phenyl-Substituted Dithienylethene Thin Films and EFISH Measurements, *J. Phys. Chem. C*, **2011**, *115*, 20425–20432.

(58) Espa, D.; Pilia, L.; Marchio`, L.; Artizzu, F.; Di Carlo, G.; Marinotto, D.; Serpe, A.; Tessore, F. and Deplano, P. A nonlinear optical active polymer film based on Pd(II) dithione/dithiolate second-order NLO chromophores, *Dalton Trans.*, **2016**, *45*, 17431–17438.

SYNOPSIS.

Interplay between donor and acceptor in dithiolene complexes promotes multiresponsive linear optical properties and proton switchable 2nd-order NLO response. Chiral acceptor ligand induces the crystallization in non-centrosymmetric space groups. Anti-Kasha proton- and silver-tunable emissions are limited to compounds bearing a quinoxaline moiety. DFT-calculations highlight these properties.